
Use of ^{11}C -PE2I PET in Differential Diagnosis of Parkinsonian Disorders

Lieuwe Appel^{1,2}, My Jonasson^{2,4}, Torsten Danfors^{1,2}, Dag Nyholm³, Håkan Askmark³, Mark Lubberink^{2,4}, and Jens Sörensen^{1,2}

¹PET Centre, Department of Medical Imaging, Uppsala University Hospital, Uppsala, Sweden; ²Section of Nuclear Medicine and PET, Department of Radiology, Oncology, and Radiation Sciences, Uppsala University, Uppsala, Sweden; ³Department of Neuroscience, Neurology, Uppsala University, Uppsala, Sweden; and ⁴Medical Physics, Uppsala University Hospital, Uppsala, Sweden

In idiopathic Parkinson disease and atypical parkinsonian disorders, central dopaminergic and overall brain functional activity are altered to different degrees, causing difficulties in achieving an unambiguous clinical diagnosis. A dual examination using ^{123}I -FP-CIT (^{123}I -*N*- ω -fluoropropyl-2 β -carbomethoxy-3 β -(4-iodophenyl)nortropine, or ^{123}I -ioflupane) SPECT and ^{18}F -FDG PET provides complementary information on dopamine transporter (DAT) availability and overall brain functional activity, respectively. Parametric images based on a single, dynamic ^{11}C -PE2I (*N*-(3-iodoprop-2E-enyl)-2 β -carbomethoxy-3 β -(4-methyl-phenyl)nortropine) scan potentially supply both DAT availability (nondisplaceable binding potential [BP_{ND}]) and relative cerebral blood flow (relative delivery [R₁]) at voxel level. This study aimed to evaluate the validity of ^{11}C -PE2I PET against the dual-modality approach using ^{123}I -FP-CIT SPECT and ^{18}F -FDG PET. **Methods:** Sixteen patients with parkinsonian disorders had a dual examination with ^{18}F -FDG PET and ^{123}I -FP-CIT SPECT following clinical routines and additionally an experimental ^{11}C -PE2I PET scan. Parametric BP_{ND} and R₁ images were generated using receptor parametric mapping with the cerebellum as a reference. T1-weighted MR imaging was used for automated definition of volumes of interest (VOI). The DAT VOIs included the basal ganglia, whereas the overall brain functional activity was examined using VOIs across the brain. BP_{ND} and R₁ values were compared with normalized ^{123}I -FP-CIT and ^{18}F -FDG uptake values, respectively, using Pearson correlations and regression analyses. In addition, 2 masked interpreters evaluated the images visually, in both the routine and the experimental datasets, for comparison of patient diagnoses. **Results:** Parametric ^{11}C -PE2I BP_{ND} and R₁ images showed high consistency with ^{123}I -FP-CIT SPECT and ^{18}F -FDG PET images. Correlations between ^{11}C -PE2I BP_{ND} and ^{123}I -FP-CIT uptake ratios were 0.97 and 0.76 in the putamen and caudate nucleus, respectively. Regional ^{11}C -PE2I R₁ values were moderately to highly correlated with normalized ^{18}F -FDG values (range, 0.61–0.94). Visual assessment of DAT availability showed a high consistency between ^{11}C -PE2I BP_{ND} and ^{123}I -FP-CIT images, whereas the consistency was somewhat lower for appraisal of overall brain functional activity using ^{123}I -FP-CIT and ^{18}F -FDG images. Substantial differences were found between clinical diagnosis and both neuroimaging diagnoses. **Conclusion:** A single, dynamic ^{11}C -PE2I PET investigation is a powerful alternative to a dual examination with

^{123}I -FP-CIT SPECT and ^{18}F -FDG PET for differential diagnosis of parkinsonian disorders. A large-scale patient study is, however, needed to further investigate distinct pathologic patterns in overall brain functional activity for various parkinsonian disorders.

Key Words: parkinsonism; dopamine transporter; DAT; overall brain functional activity; PET; SPECT

J Nucl Med 2015; 56:234–242
DOI: 10.2967/jnumed.114.148619

Parkinsonian disorders are neurodegenerative and chronic brain diseases including idiopathic Parkinson disease (IPD) and atypical parkinsonian disorders, such as multiple-system atrophy (MSA), progressive supranuclear palsy and corticobasal degeneration, and dementia with Lewy bodies. Although the clinical progression and pathology differ between parkinsonian disorders, there are clear difficulties in achieving an unambiguous diagnosis based solely on clinical features of parkinsonism, particularly in the elderly and in patients at an early stage of the disease (1–3). Furthermore, IPD-like symptoms may also originate from cerebrovascular disease (vascular parkinsonism) or neurofunctional disorders initiated by medication, drugs of abuse, and posttrauma or psychogenic conditions (4). Consequently, there are profound challenges in establishing the primary cause of parkinsonism. For the individual patient, an uncertain diagnosis of parkinsonism can lead to unnecessary medical investigations and inappropriate therapies with undesired side effects while expanding costs for the health care system.

Functional molecular imaging methods such as SPECT and PET, using different radiotracers, can aid in differentiation between parkinsonian disorders and their mimics because central dopaminergic and overall brain functional activity are altered differently (4–7). SPECT and the commercially available radiotracers ^{123}I -FP-CIT (^{123}I -*N*- ω -fluoropropyl-2 β -carbomethoxy-3 β -(4-iodophenyl)nortropine, or ^{123}I -ioflupane [DaTscan; GE Healthcare]) or β -CIT (2 β -carbomethoxy-3 β -(4-iodophenyl)nortropine [DOPASCAN; MAP Medical Technologies]) have been used widely to investigate dopamine transporter (DAT) availability (8). Further, SPECT with commercial $^{99\text{m}}\text{Tc}$ -labeled compounds such as ethyl cysteine dimer (ECD; NeuroLite; Lantheus Medical Imaging) and hexamethylpropyleneamine oxime (HMPAO; Ceretec; GE Healthcare) has been used to examine alterations in the brain's overall function, mirroring

Received Sep. 16, 2014; revision accepted Dec. 17, 2014.
For correspondence or reprints contact: Lieuwe Appel, PET Centre, Department of Medical Imaging, Uppsala University Hospital, S-751 85 Uppsala, Sweden.
E-mail: lieuwe.appel@akademiska.se.
Published online Jan. 15, 2015.
COPYRIGHT © 2015 by the Society of Nuclear Medicine and Molecular Imaging, Inc.

metabolic activity and cerebral blood flow, respectively (9). For the same purpose, ^{18}F -FDG PET can support the discrimination of parkinsonian disorders based on distinct regional patterns of changes in cerebral ^{18}F -FDG use (10–12) and, thus, altered overall brain functional activity. In addition, various PET radioligands have been used to evaluate dopaminergic function (7,13). Although both SPECT and PET investigations have been partly successful in establishing the primary causes of parkinsonism, further improvement is still needed with respect to data quality, radiation dose, and scanning logistics.

The cocaine derivative PE2I (*N*-(3-iodoprop-2E-enyl)-2 β -carbomethoxy-3 β -(4-methyl-phenyl)nortropane) binds highly selectively and specifically to DAT and offers a high potential for in vivo exploration of DAT function (14). PE2I is structurally related to β -CIT and FP-CIT SPECT radioligands, but in contrast to PE2I, the CIT compounds bind to serotonin and norepinephrine transporters as well (15,16). The PET radioligand ^{11}C -PE2I has been previously used both in research studies (17,18) and in clinical trials (19,20). A kinetic modeling approach using a reference tissue model has been demonstrated to result in reliable and reproducible DAT estimates (21,22). Recently, our group validated and reported generation of parametric relative delivery (R_1) and non-displaceable binding potential (BP_{ND}) ^{11}C -PE2I images, reflecting relative cerebral blood flow (CBF) and DAT availability, respectively, in data from subjects with and without neurodegeneration (23).

Currently, the routine investigation of parkinsonian disorders at our hospital consists of a dual examination: ^{123}I -FP-CIT SPECT and ^{18}F -FDG PET imaging. The ^{123}I -FP-CIT SPECT examination is used to discriminate between patients with and without dopaminergic parkinsonism based on DAT availability, whereas ^{18}F -FDG PET is applied to examine overall brain functional activity for differentiation of parkinsonian disorders. Our hypothesis was that ^{11}C -PE2I BP_{ND} and R_1 images are congruent with ^{123}I -FP-CIT SPECT and ^{18}F -FDG PET, respectively, and that a single dynamic ^{11}C -PE2I PET investigation can provide a diagnosis equivalent to that from the current dual examination. The main purpose was, therefore, to investigate the validity of ^{11}C -PE2I PET against the current routine imaging-based evaluation of parkinsonian disorders in terms of image information and visual inspection of images in a clinical setting.

MATERIALS AND METHODS

Participants

Nineteen patients (11 women and 8 men) with parkinsonian disorders were recruited by the Department of Neurology at Uppsala University Hospital. The main inclusion criterion was that each patient had undergone or been referred for the routine dual imaging investigations using ^{18}F -FDG PET and ^{123}I -FP-CIT SPECT. Further, selection of patients for ^{11}C -PE2I imaging was based on medical records and an interview with an appraisal of health status, lifestyle, and medication. Finally, the time point of the ^{11}C -PE2I scan had to differ by no more than 1 y from the other scans.

Before the data analysis, it appeared that 1 woman had not undergone all imaging assessments within 1 y and that 2 men had no evaluable ^{11}C -PE2I PET scan because of excessive movement. Therefore, the presented data comprised 16 patients with parkinsonism (10 women and 6 men; mean age \pm SD, 69 ± 6 y; mean body weight, 67 ± 11 kg) experiencing symptoms for less than approximately 5 y on average. The clinical rationale for referral to routine imaging investigations was an uncertain-to-poor response to medica-

tion, as well as symptoms and clinical findings not typical of IPD. Patient characteristics are described in Table 1.

Imaging Procedures

The ^{11}C -PE2I PET scans were acquired on an ECAT HR+ scanner (Siemens/CTI). For attenuation correction, a 10-min transmission scan (2-dimensional mode) was obtained, using 3 retractable ^{68}Ge line sources. After the transmission scan, 350–400 MBq of ^{11}C -PE2I were administered intravenously as a rapid bolus in the subject's arm. Simultaneously, a dynamic emission scan was started (3-dimensional mode) using a scanning protocol comprising 22 frames with increasing frame duration (4×60 s, 2×120 s, 4×180 s, 12×300 s) and a total scanning time of 80 min. Imaging data were reconstructed with ordered-subsets expectation maximization (6 iterations; 8 subsets) and a 4-mm Hanning filter, after implementation of all appropriate corrections, such as those for photon attenuation, random coincidences, scattered radiation, dead time, and physical decay of the radioisotope.

^{18}F -FDG PET was performed on a Discovery STE PET/CT scanner (GE Healthcare), approximately 35 min after intravenous administration of 3 MBq of ^{18}F -FDG per kilogram of body weight. For the emission scan, a 10- or 20-min protocol was used, comprising 2 or 4 frames, respectively, with a 5-min duration. A low-dose CT scan was obtained for attenuation correction. Data reconstruction was similar to that for ^{11}C -PE2I.

^{123}I -FP-CIT scanning was performed with a dual-head γ camera (E.CAM; Siemens Medical Systems) equipped with high-resolution collimators, after intravenous administration of 185 MBq of ^{123}I -FP-CIT 3–6 h before the start of scanning. The total time of acquisition was 30 min (30 s per frame for 60 views per detector). Data were reconstructed with ordered-subsets expectation maximization including attenuation and scatter correction, and implementation of resolution recovery, followed by use of a gaussian filter (0.7 cm in full width at half maximum).

All participants also underwent T1-weighted MR imaging (3-dimensional sensitivity encoding) on a 1.5-T Achieva scanner (Philips Healthcare). This scan provided structural information with a high resolution, to be used to define regions of interest.

The subjects fasted for at least 4 h before scanning. For ethical reasons, we did not interfere with the medication of the patients.

The timing of the scans is summarized in Table 1. Before the data analysis, we found that for subject 13 the interval between ^{11}C -PE2I and ^{123}I -FP-CIT SPECT differed by about 18 mo, whereas this interval was about 1 y for the ^{11}C -PE2I and ^{18}F -FDG scans. On the basis of clinical symptoms and disease duration, this subject was considered stable for DAT function and consequently was included.

Image Analysis

Methods for voxel-level analysis of dynamic ^{11}C -PE2I scans have been previously validated and reported (19). Following this methodology, the ^{11}C -PE2I images were realigned to adjust for interframe patient movements using VOIager software (GE Healthcare). Then, the T1-weighted MR images were coregistered with the realigned PET images using an ^{11}C -PE2I early summation image (0–3 min), to achieve equivalent image positions. Finally, parametric images were generated from the ^{11}C -PE2I scan using the preferred basis function implementation (receptor parametric mapping) of the simplified reference tissue model, with the cerebellum as a reference region (24,25). The parametric ^{11}C -PE2I BP_{ND} images showed specific binding of ^{11}C -PE2I to DAT directly proportional to DAT density (availability). The parametric ^{11}C -PE2I R_1 images demonstrated relative CBF.

For the ^{18}F -FDG scan, the frames were realigned to adjust for interframe movements using VOIager software, and subsequently a summation image was made across frames. The ^{18}F -FDG summation image was coregistered with the ^{11}C -PE2I R_1 images to establish the same

TABLE 1
Patient Characteristics at Time of ¹¹C-PE2I Scan

Subject	Sex	Age (y)	H&Y staging	Duration (y)	Parkinson treatment		Scanning interval (d)	
					Drug	Daily dose (mg)	PE2I-DAT	PE2I-FDG
1	F	74	3	4	L-dopa	600	282	-218
2	F	73	4	7	L-dopa	1,200	-92	-92
4	M	63	3	6	Pramipexole	1.05	104	105
					L-dopa	800		
5	F	77	3	8	Ropinirole	10	82	82
					L-dopa	500		
6	F	60	3	12	Quetiapine	200	-1	-1
7	M	70	3	10	L-dopa	600	184	188
8	F	65	3	4	None		23	152
9	F	66	3	3	L-dopa	300	-1	326
					Pramipexole	2.1		
10	M	77	5	6	L-dopa	500	-16	-16
					Pramipexole	0.54		
11	F	67	2	2	L-dopa	250	-37	-37
12	M	79	2	4	L-dopa	400	-36	-36
13	F	71	2	4	L-dopa	600	373	628
14	M	71	3	3	L-dopa	400	-1	-1
15	M	58	2	1.5	L-dopa	500	154	202
16	F	67	3	2	None		-1	-1
19	F	69	1	1.5	L-dopa	400	-1	-1

H&Y = Hoehn and Yahr; PE2I-DAT = days between ¹¹C-PE2I PET and ¹²³I-FP-CIT SPECT; PE2I-FDG = days between ¹¹C-PE2I PET and ¹⁸F-FDG PET.

position for all images. Then, the realigned ¹⁸F-FDG summation image was normalized to the average radioactivity concentrations in cerebellum.

The ¹²³I-FP-CIT SPECT scan was analyzed following routine procedures for DaTSCAN (GE Healthcare). Coregistration with PET and MR images was not applied because of lack of structural information in ¹²³I-FP-CIT images.

Volumes of Interest (VOIs)

For the PET data, an automated probabilistic template, as implemented in the PVElab software (26), was used for definition of VOIs across slices on the coregistered MR images. Then, the VOIs were transferred to the parametric ¹¹C-PE2I R₁ and BP_{ND} as well as the normalized ¹⁸F-FDG images.

The considered DAT VOIs included the basal ganglia (bilaterally, the caudate nucleus and putamen), regions with a recognized high DAT density, and following our routine evaluations of ¹²³I-FP-CIT SPECT. The comparison of the parametric ¹¹C-PE2I R₁ images and the normalized ¹⁸F-FDG images was based on various VOIs across the brain, as alterations of overall brain functional activity differ between parkinsonian disorders. The set of VOIs comprised cortical regions in the frontal, temporal, parietal, occipital, and insular lobes, as well as subcortical regions in the basal ganglia, limbic system, and thalamus. In addition, the midbrain as well as gray and white matter were considered.

For the ¹²³I-FP-CIT images, the basal ganglia VOIs were generated using an automated template (27) belonging to the BRASS software (version 3.6; Hermes Medical Solutions), resulting in regional uptake values normalized to the occipital cortex. All was done using the same software.

Data Evaluation

Quantitative values for each VOI were obtained by retrieving average regional voxel values from the generated parametric ¹¹C-PE2I R₁ and BP_{ND} images as well as from the normalized ¹⁸F-FDG image. For ¹²³I-FP-CIT images, the uptake ratios were used as generated by the BRASS software. Agreement between methods in terms of DAT availability and overall brain functional activity was evaluated using Pearson correlation and orthogonal regression analysis, assuming equal error variances of the compared variables. For DAT availability, orthogonal regressions were computed for both the putamen and the caudate nucleus separately. Concerning overall brain functional activity, orthogonal regression analyses were implemented for a cluster of VOIs across the brain including anterior cortical regions (cingulate, frontal gyrus), posterior cortical regions (occipital cortex, parietal cortex, somatosensory-motor cortex), basal ganglia (caudate nucleus, putamen), or limbic regions (amygdala, hippocampus, hypothalamus, thalamus).

Comparison of Patient Diagnoses

Parkinsonism was diagnosed on the basis of both clinical and neuroimaging data to further investigate the validity of ¹¹C-PE2I in a clinical setting. Two movement disorders specialists who were masked to the imaging data established a clinical diagnosis by following clinical routines and accepted criteria (28–33). In turn, 2 masked nuclear medicine specialists independently evaluated the imaging data visually on the basis of specific pathologic patterns of glucose metabolism as reported for various parkinsonian disorders (6,11,12). The imaging-based patient diagnosis comprised the most probable type of

parkinsonism and was determined for both the novel evaluation using ^{11}C -PE2I BP_{ND} and R_1 images and the routine evaluation using ^{123}I -FP-CIT SPECT and ^{18}F -FDG PET images. First, DAT availability was rated as normal or abnormal using either ^{11}C -PE2I BP_{ND} or ^{123}I -FP-CIT images; then, overall brain functional activity was characterized as normal or abnormal using either ^{11}C -PE2I R_1 or ^{18}F -FDG images. The appraisal of DAT availability and overall brain functional activity resulted in a single imaging-based diagnosis for each patient in each dataset. To avoid dependency between these assessments, the individual records of both datasets were randomized in different orders and evaluated on different days. Thereafter, the imaging-based diagnoses obtained by each nuclear medicine specialist were compared on a separate occasion. In cases of discrepancy in diagnosis, the nuclear medicine specialists discussed the case together to reach a consensus.

Ethical Statement

The study was conducted in accordance with the Declaration of Helsinki and approved by the local ethics and radiation safety committees. After receiving a complete description of the study, and before the study began, each patient gave written informed consent to participate.

RESULTS

DAT Availability

Parametric ^{11}C -PE2I BP_{ND} images and ^{123}I -FP-CIT uptake images, illustrating DAT availability, are presented for various parkinsonian disorders in Figure 1. The most probable diagnosis was based solely on PET images from either parametric ^{11}C -PE2I BP_{ND} and R_1 or the dual investigation with ^{123}I -FP-CIT SPECT and ^{18}F -FDG PET.

The ^{123}I -FP-CIT images displayed information equivalent to that from the ^{11}C -PE2I BP_{ND} images, with the highest uptake being in striatal structures. Furthermore, this sample of images illustrated for both methods the potency to discriminate visually between subjects with and without dopaminergic parkinsonism, cases A–C and D–E, respectively. However, the resolution was superior for the BP_{ND} images, allowing visual discernment of the putamen and caudate nucleus for cases with the highest DAT availability (D and E). In part, the ^{123}I -FP-CIT images may also display affinity for serotonin and norepinephrine transporters.

Overall Brain Functional Activity

Parametric ^{11}C -PE2I R_1 and normalized ^{18}F -FDG images, depicting overall brain functional activity, are shown in Figure 2. As for the images in Figure 1, the most probable diagnosis was based entirely on DAT availability and overall brain functional activity for both evaluations.

The different cases show that visually equivalent information was obtained with ^{11}C -PE2I R_1 and ^{18}F -FDG images. On the basis of DAT availability, 2 cases did not indicate dopaminergic parkinsonism (D and E). However, overall brain functional activity was clearly abnormal in one case, with reduced cortical glucose metabolism/relative CBF pointing toward vascular parkinsonism (D). In contrast, the other subject showed normal overall brain functional activity (E) regarding both glucose metabolism and relative CBF. Three cases showed a significant decrease in DAT availability (A–C), and on the basis of images reflecting overall brain functional activity, the distinct patterns were recognized as typical of IPD, MSA, and progressive supranuclear palsy. For IPD, a prominent, enhanced glucose metabolism/relative CBF was anticipated bilaterally in the putamen, which was congruent with case A. Supporting features were a decrease in glucose metabolism/relative CBF in frontal and parietal regions. Bilaterally low glu-

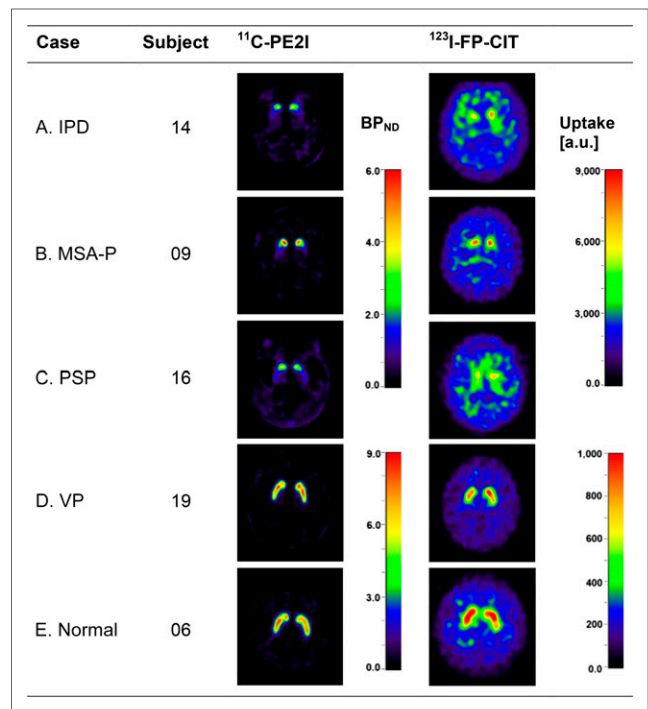


FIGURE 1. Parametric images of ^{11}C -PE2I BP_{ND} compared with ^{123}I -FP-CIT uptake images, illustrating DAT availability in patients diagnosed with different types of parkinsonism. a.u. = arbitrary unit; MSA-P = MSA with suggested predominated parkinsonism; normal = no notable deviation in dopaminergic function; VP = vascular parkinsonism.

cose metabolism in the putamen elucidated cases typical of MSA, which was consistent with the decrease in relative CBF (case B). Because cerebellar neurodegeneration was not evident, this patient was categorized as having MSA with suggested predominant parkinsonism. Further, increased glucose metabolism/relative CBF was observed in the thalamus and the posterior cortical areas, especially the occipital cortex. Finally, case C was diagnosed as progressive supranuclear palsy on the basis of the reduced glucose metabolism/relative CBF in the medial frontal cortex and mesencephalon, as well as enhanced glucose metabolism/relative CBF in the inferior temporal and parietal cortex.

One patient (patient 4) was diagnosed as having MSA with atrophy related to the cerebellum (Fig. 3). Both ^{11}C -PE2I R_1 and ^{18}F -FDG images, illustrating overall brain functional activity, revealed a noteworthy degeneration of the cerebellar cortex. However, other glucose metabolism/relative CBF patterns were visually similar to those observed for the patient with MSA with suggested predominant parkinsonism (Fig. 2, case B). In addition, there was visually no indication that the DAT availability was different between the two types of MSA.

Relationship Between ^{123}I -FP-CIT and ^{11}C -PE2I BP_{ND} Values

The correlations between normalized ^{123}I -FP-CIT uptake values and ^{11}C -PE2I BP_{ND} values were 0.96 and 0.76 for the putamen and caudate nucleus, respectively. Plots of putamen and caudate nucleus data are depicted in Figure 4. For both evaluation methods, the data for the putamen showed an apparent differentiation in a majority of subjects having relatively small values (≤ 1.5) and a minority of subjects having relatively high values (A). For the caudate nucleus (B), such a differentiation was less evident. Orthogonal regression analyses showed that the slopes of the regression

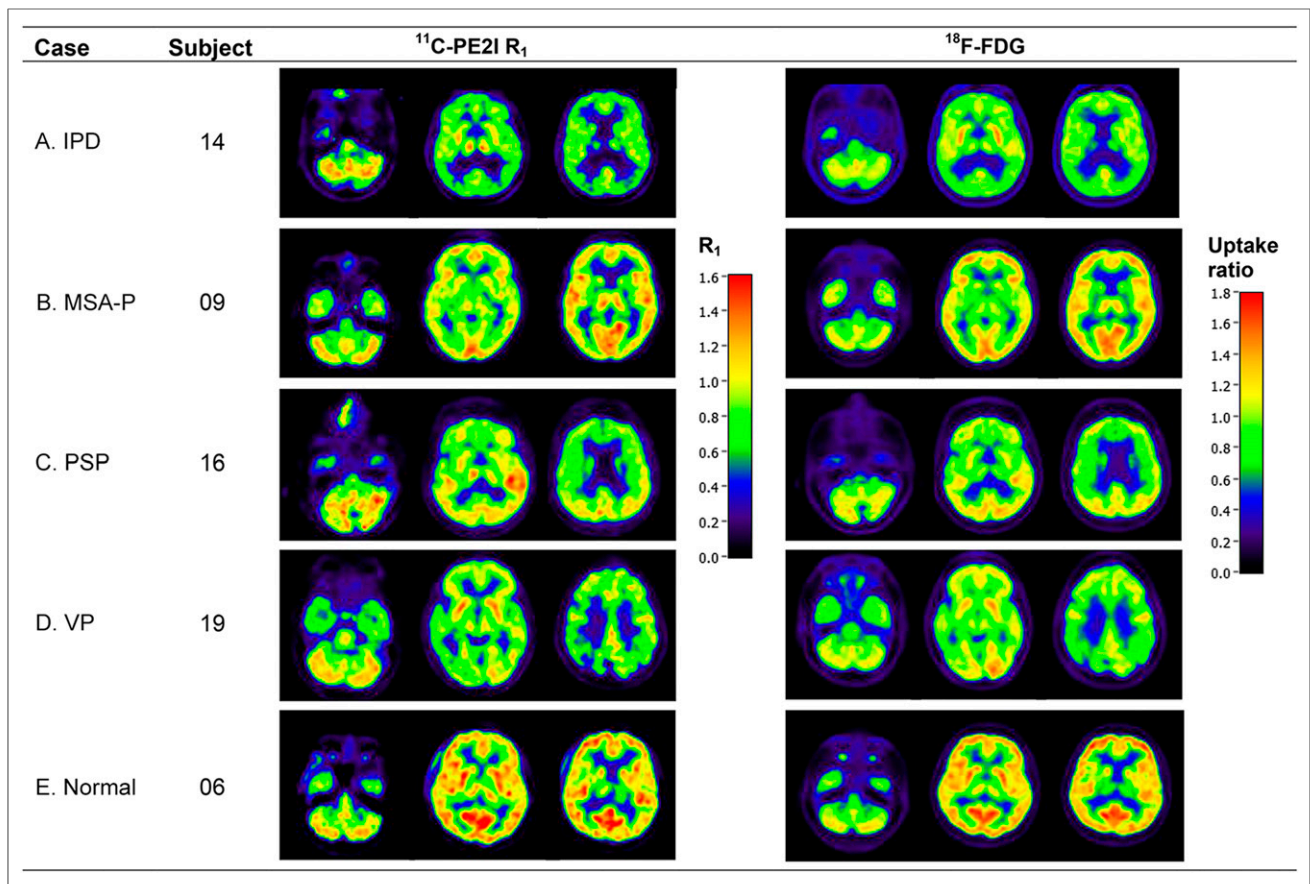


FIGURE 2. Parametric images of $^{11}\text{C-PE2I}$ relative delivery (R_1) compared with $^{18}\text{F-FDG}$ images normalized to cerebellum, illustrating overall brain functional activity in patients diagnosed with different types of parkinsonism. MSA-P = MSA with suggested predominant parkinsonism; normal = no notable deviation in overall brain functional activity; PSP = progressive supranuclear palsy; VP = vascular parkinsonism.

curves differed significantly from unity for both the putamen and the caudate nucleus ($P < 0.05$). The intercept deviated significantly from zero for the caudate nucleus ($P < 0.05$) but not for the putamen.

Relationship Between $^{18}\text{F-FDG}$ and $^{11}\text{C-PE2I } R_1$ Values

Correlations between normalized $^{18}\text{F-FDG}$ uptake values and $^{11}\text{C-PE2I } R_1$ values are given in Table 2 for various brain regions. Most correlations were greater than 0.75, and the highest correlations were found for cortical regions.

Orthogonal regression analyses showed a high relationship between normalized $^{18}\text{F-FDG}$ uptake values and $^{11}\text{C-PE2I } R_1$ values for clusters of data for the anterior cortical regions, posterior cortical regions, and limbic regions, whereas a slightly lower correlation was found for the basal ganglia (Fig. 5). The slope of the regression curves was greater than 1 for anterior cortical regions ($P < 0.05$) and limbic regions, whereas the slopes were less than 1 for posterior cortical regions and the basal ganglia (both $P < 0.05$). In all cases, the intercepts did not significantly differ from zero.

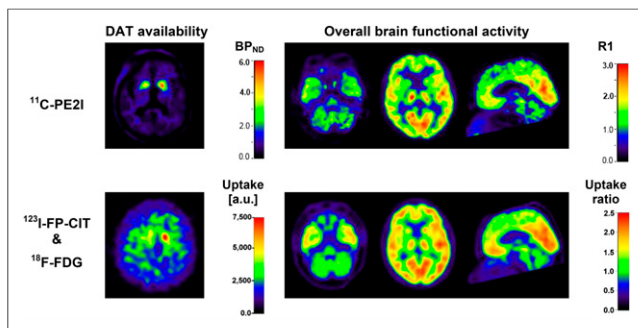


FIGURE 3. Parametric images of $^{11}\text{C-PE2I}$ relative delivery (R_1) and BP_{ND} compared with $^{123}\text{I-FP-CIT}$ and $^{18}\text{F-FDG}$ images, illustrating DAT availability and overall brain functional activity in patient 4, diagnosed MSA with atrophy related to cerebellum. a.u. = arbitrary unit.

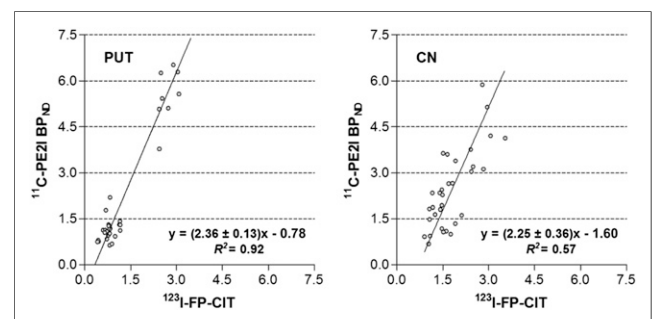


FIGURE 4. Relationship between normalized uptake of $^{123}\text{I-FP-CIT}$ and $^{11}\text{C-PE2I } \text{BP}_{\text{ND}}$ for putamen (PUT) and caudate nucleus (CN).

TABLE 2
Correlation Between Normalized ^{18}F -FDG Uptake Values and ^{11}C -PE2I R_1 Values

Brain region of interest		<i>r</i>
Structure	Volume (26)	
Whole brain	Gray matter	0.76
	White matter	0.69
Frontal lobe	Frontal gyrus (superior, medial-inferior)	0.80
	Orbital frontal cortex	0.75
	Dorsolateral prefrontal cortex	0.75
	Ventrolateral prefrontal cortex	0.82
	Anterior cingulate gyrus	0.85
	Posterior cingulate gyrus	0.93
Temporal lobe	Lateral temporal cortex (superior, medial-inferior)	0.76
Parietal lobe	Parietal cortex	0.94
Occipital lobe	Occipital cortex	0.88
Insular lobe	Insula	0.79
	Somatosensory and motor cortex	0.74
Basal ganglia	Caudate nucleus, putamen	0.81
Limbic regions	Amygdala, hippocampus, hypothalamus	0.68
	Thalamus	0.76
Midbrain	Midbrain	0.61

n = 15 (1 subject was disregarded because of significant neurodegeneration in cerebellum [Fig. 3]).

Comparison of Patient Diagnoses

Diagnoses of parkinsonism, based on 3 different sources of information, are presented in Table 3.

The visual assessment of DAT availability showed a high consistency between ^{11}C -PE2I BP_{ND} and ^{123}I -FP-CIT images, with

only one discrepancy. On the basis of both DAT availability and overall brain functional activity, there were 4 discrepancies in patient diagnosis between the datasets, including ^{11}C -PE2I PET and BP_{ND} or normalized ^{18}F -FDG PET and ^{123}I -FP-CIT SPECT.

The clinical diagnosis differed in 9 and 8 patients compared with imaging-based diagnoses using either ^{11}C -PE2I BP_{ND} and R_1 images or ^{123}I -FP-CIT and ^{18}F -FDG images, respectively. Mean and median age, Hoehn and Yahr score, and disease duration were similar in the groups with and without consistency between the imaging-based and clinical diagnoses.

DISCUSSION

In this clinical study, the validity of a single dynamic ^{11}C -PE2I PET scan was evaluated for discrimination of different types of parkinsonism. For this purpose, parametric BP_{ND} and R_1 images were compared with a dual examination using ^{123}I -FP-CIT and ^{18}F -FDG PET to examine dopaminergic and overall brain functional activity, respectively. This study confirmed that ^{11}C -PE2I PET R_1 and BP_{ND} images comprised information that was equivalent—in terms of specific pathologic patterns and moderate to high correlations—to the combination of ^{123}I -FP-CIT SPECT and ^{18}F -FDG PET. Recently, a similar result was reported (34) for ^{11}C -Pittsburgh compound B PET scans using parametric R_1 and BP_{ND} images for assessment of relative CBF and regional amyloid- β depositions, respectively, in patients with dementia. Altogether, the results of the current study provide sufficient evidence that a single dynamic ^{11}C -PE2I PET scan can be used for differential diagnosis of parkinsonian disorders.

The comparison between ^{11}C -PE2I BP_{ND} and ^{123}I -FP-CIT images revealed a high consistency in particular patterns of DAT

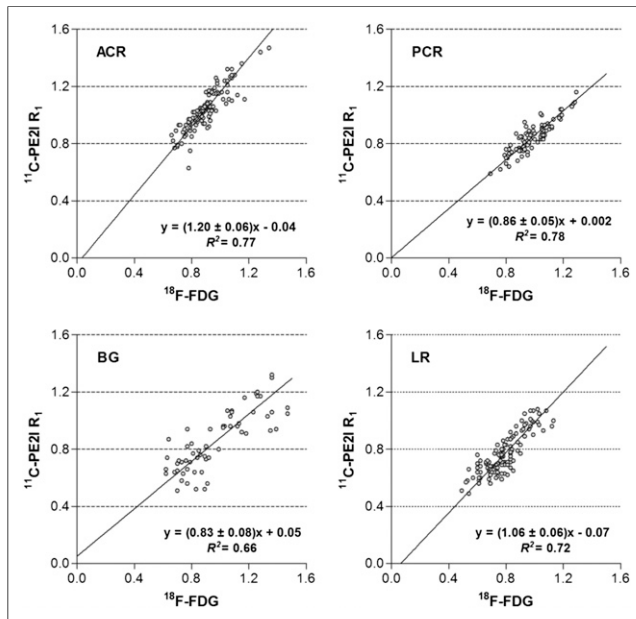


FIGURE 5. Relationship between normalized uptake of ^{18}F -FDG and ^{11}C -PE2I R_1 for anterior cortical region (ACR), posterior cortical region (PCR), basal ganglia (BG), and limbic region (LR).

TABLE 3
Comparison of Diagnosis Based on Visual Assessment of Neuroimaging Data and Clinical Assessment

Subject	Information source for diagnosis				
	A. Parametric images of ^{11}C -PE2I		B. Normalized ^{123}I -FP-CIT and ^{18}F -FDG images		C. Clinical data
	BP _{ND}	Both R ₁ and BP _{ND}	^{123}I -FP-CIT	Both scans	
1	↓	MSA	↓	MSA	Probable MSA
2	↓	MSA	↓	MSA	Probable MSA
4	↓	MSA	↓	MSA	Probable MSA
5	↓	IPD*	↓	PSP*	Possible MSA†‡
6	→	Normal	→	Normal	Possible PSP†‡
7	↓	IPD	↓	IPD	Probable IPD
8	→	Normal*	→	VP*	CBD†‡
9	↓	MSA	↓	MSA	Possible IPD†‡
10	→	VP*	↓	IPD*	CBD†‡
11	↓	IPD	↓	IPD	Possible DLB†‡
12	↓	IPD	↓	IPD	Probable IPD
13	↓	PSP*	↓	IPD*	Probable IPD†
14	↓	IPD	↓	IPD	Probable MSA†‡
15	↓	IPD	↓	IPD	Probable IPD
16	↓	PSP	↓	PSP	Probable PSP
19	→	VP	→	VP	Possible IPD†‡

*Difference in diagnosis between evaluations of neuroimaging data (A and B).

†Difference in diagnosis based on data of A and C.

‡Difference in diagnosis based on data from B and C.

PSP = progressive supranuclear palsy; Normal = no significant deviation in dopaminergic and overall function; VP = vascular parkinsonism; CBD = corticobasal degeneration; DLB = dementia with Lewy bodies; ↓ = significant decrease in observed level of DAT availability; → = no notable deviation from normal.

^{11}C -PE2I BP_{ND} and ^{123}I -FP-CIT SPECT images reflect DAT availability, whereas ^{11}C -PE2I R₁ and ^{18}F -FDG PET images mirror overall brain functional activity.

availability for parkinsonian disorders. A high correlation between both assessments was found for the putamen, whereas the correlation was moderate for the caudate nucleus. In both cases, the slopes of the regression curves were significantly greater than 1, indicating an extended range of ^{11}C -PE2I BP_{ND} values compared with ^{123}I -FP-CIT values. Visual appraisal of DAT availability showed high agreement between the ^{123}I -FP-CIT and ^{11}C -PE2I BP_{ND} datasets. On the basis of these results, it is anticipated that the ^{11}C -PE2I BP_{ND} values are at least as reliable as ^{123}I -FP-CIT values in discrimination of normal from abnormal DAT function in parkinsonian disorders.

^{11}C -PE2I R₁ images, depicting relative CBF, were highly consistent with ^{18}F -FDG images, displaying glucose metabolism, which corresponded well with results in dementia patients (34). Typical pathologic patterns in overall brain functional activity, showing presynaptic neuronal dysfunction and degeneration, could be recognized for different parkinsonian disorders in both ^{11}C -PE2I R₁ and ^{18}F -FDG images. Correlations between ^{11}C -PE2I R₁ and ^{18}F -FDG values varied from moderate to high with a tendency to be slightly higher in cortical regions than in subcortical regions. The orthogonal regression analyses also indicated minor differences between regions. These results may be due in part to regional differences in relative CBF and glucose metabolism (35),

which show a greater range in cortical regions, and to the larger size of the cortical and clustered VOIs, resulting in more accurate values.

A visual assessment of the most probable diagnosis, using neuroimaging with assessment of both DAT availability and overall brain functional activity, showed a discrepancy of 25% between the novel evaluation using parametric images of ^{11}C -PE2I and the routine evaluation using ^{123}I -FP-CIT SPECT and ^{18}F -FDG PET. The evaluation revealed that 3 of these patients (5, 10, and 13) had in common an uncertain to poor response to medication, whereas patient 8 had no medication. Two of these cases (patients 8 and 10) had at least one assessment of normal DAT function, whereas both had a clinical diagnosis of corticobasal degeneration. As alterations in DAT and overall brain functional activity may become more evident at a later stage, it would be desirable to repeat the same measurements 6–18 mo later. Both of the other 2 cases (patients 5 and 13) showed an abnormality in DAT and overall brain functional activity, resulting in imaging-based diagnoses of IPD and progressive supranuclear palsy. However, for patient 13, the discrepancy in results depended most likely on the timing of the scans since the ^{18}F -FDG scan was conducted about 12 mo before the ^{11}C -PE2I PET scan. Further, evident pathologic differences in overall brain functional activity images were noticed by the nuclear

medicine specialists. In contrast, for patient 5, all investigations were performed within 3 mo, and the same patterns were found for the novel and routine evaluations. For both cases, however, the poor effect of medication speaks rather for non-IPD parkinsonism than IPD, which may become more obvious at later stages, and additional imaging of overall brain functional activity may confirm this hypothesis.

After the neuroimaging evaluation (either routine or novel), in about half of patients the clinical diagnosis was not consistent with the imaging results. This outcome was not unexpected, as most of the referred patients either had a poor response to medication or had symptoms and findings not typical of IPD. Further, in a clinicopathologic study the accuracy of the clinical diagnosis of IPD did not exceed 76% (1), whereas in about 52% of patients with parkinsonism the clinical diagnosis was changed after ^{123}I -FP-CIT SPECT imaging (3). Those results emphasize the value of novel imaging approaches for differential diagnosis of Parkinsonian disorders. However, further comparison of ^{11}C -PE2I R_1 with ^{18}F -FDG in an extensive prospective clinical study is needed to extend insights and experience in the assessment of overall brain functional activity and to develop a generic approach with a high degree of diagnostic consensus. Age-matched control material would further help discriminate the causes of parkinsonism, especially for implementation of support from computerized evaluations.

One patient showed significant cerebellar neurodegeneration and was identified as having MSA with atrophy related to the cerebellum (Fig. 3). As a consequence, regional normalized ^{18}F -FDG uptake values, as well as ^{11}C -PE2I R_1 values, were significantly above the average. This outlier could potentially affect the correlation and regression analyses in this relatively small sample and was, therefore, excluded. Importantly, the generation of parametric ^{11}C -PE2I R_1 and BP_{ND} images may also be affected when cerebellum is used as the reference region. Supervised clustering methods for extracting reference tissue curves (36) may be used to overcome a potential bias of ^{11}C -PE2I R_1 and BP_{ND} estimates, and an implementation for this kind of data is under investigation.

A clinical implementation of ^{11}C -PE2I PET for differential diagnosis of parkinsonian disorders has several advantages over ^{123}I -FP-CIT SPECT and ^{18}F -FDG PET imaging with respect to data quality, radiation dose, and scanning logistics. One advantage is that PET images have a higher resolution than SPECT images. The data quality is further improved by the use of established kinetic models for generation of parametric images, which allow valid voxelwise analysis. In addition, the radioligand ^{11}C -PE2I binds highly selectively to DAT, whereas ^{123}I -FP-CIT SPECT also has high affinity for serotonin transporters and moderate affinity for norepinephrine transporters (15), causing an overestimation of DAT availability (16). When using solely a single ^{11}C -PE2I PET scan, the radiation dose is reduced by approximately 70% from about 8.4 mSv for the combination of ^{123}I -FP-CIT SPECT (8) and ^{18}F -FDG PET (37) to about 2.5 mSv for ^{11}C -PE2I PET (38). From a patient perspective, a single scan is more convenient than a dual examination. Further, the preparation time before scanning can be up to 6 h for a ^{123}I -FP-CIT SPECT scan but less than 30 min for an ^{11}C -PE2I scan. One disadvantage is that from a kinetic modeling perspective an ^{11}C -PE2I scan should be at least 70 min (21) to reliably quantify striatal DAT, which certainly increases the risk for significant movement or for the patient's being unable to complete the examination. Currently, we are investigating methods for shortening the total examination time. Another disadvantage is that ^{11}C -PE2I has to be produced in a PET facility with its own

production capacity because of the limited half-life of ^{11}C . In contrast to ^{18}F -tracers, ^{11}C -PE2I can therefore not be transported over long distances. On the other hand, differential diagnosis of parkinsonism used to take place at specialized hospitals, which often have, besides a PET scanning facility, their own tracer production facility at good-manufacturing-practice level. At our facility, ^{11}C -PE2I production was robust and yielded batches for scanning 2–4 patients. Balancing the pros and cons of the implementation of ^{11}C -PE2I for differential diagnosis of parkinsonian disorders, we anticipate that the advantages strongly overrule the disadvantages in a clinical setting with a good-manufacturing-practice tracer production facility.

The present study was subject to some limitations. One was the study population, which was restricted to 16 patients. The complexity of a study with 4 imaging occasions was demanding for this category of patients. Further, the referred patients were extremely challenging in terms of health status and diagnosis and were not representative of the total population with parkinsonism. Most of the patients were diagnosed as having IPD or MSA, with other disorders being constrained to a single case or not represented at all. In addition, the diagnoses should be considered as possible or probable clues of the clinical cases, as the patients' parkinsonism may be further elucidated at later stages and only pathologic data can confirm the diagnoses. Further, neuroimaging examinations were performed on different occasions, and disease progression might have affected the comparisons. However, we judged that a 12-mo imaging period was reasonable from both a recruitment perspective and an evaluation perspective. Finally, medication of the patients could have influenced the results. For example, most patients were taking dopaminergic medication (Table 1), which might have resulted in enhanced DAT availability (39). Some patients received depression medication, which may cause an underestimation of DAT availability, especially ^{123}I -FP-CIT SPECT values (16,40). The impact of medication on the results should, however, be limited as every patient was his or her own control. Despite some limitations, the present study supplied valuable information on the feasibility of the clinical use of ^{11}C -PE2I for discrimination of parkinsonian disorders, and some critical issues will be addressed in later studies.

CONCLUSION

This study provided sufficient evidence that parametric ^{11}C -PE2I images can be clinically used to evaluate parkinsonian disorders. ^{11}C -PE2I BP_{ND} PET images, mirroring dopaminergic function through DAT availability, were superior to ^{123}I -FP-CIT SPECT images both in image quality and in data quality, confirming that ^{11}C -PE2I can substitute for ^{123}I -FP-CIT in DAT assessments. Furthermore, ^{11}C -PE2I R_1 images, depicting overall brain functional activity, correlated strongly with ^{18}F -FDG images, reflecting the interrelationship of relative CBF and glucose metabolism. On visual inspection, a discrepancy of 25% was found between the imaging-based diagnosis using parametric images of ^{11}C -PE2I and the one using ^{123}I -FP-CIT SPECT and ^{18}F -FDG PET. The distinct alterations of overall brain functional activity, observed in ^{11}C -PE2I R_1 images, should be further investigated in a large-scale prospective study on patients with various parkinsonian disorders to develop a generic approach with a high degree of diagnostic consensus.

A single, dynamic ^{11}C -PE2I PET investigation is a powerful alternative to the combination of ^{123}I -FP-CIT SPECT and ^{18}F -FDG PET as a clinical routine for a differential diagnosis of parkinsonian disorders.

DISCLOSURE

The costs of publication of this article were defrayed in part by the payment of page charges. Therefore, and solely to indicate this fact, this article is hereby marked "advertisement" in accordance with 18 USC section 1734. This work was in part financed by grants from Uppsala University Hospital, the Swedish Parkinson Foundation, and the Swedish Research Council. No other potential conflict of interest relevant to this article was reported.

ACKNOWLEDGMENTS

We thank the patients for their participation in the study and the staff at the departments for PET, NM, MRI, and Medical Physics at Uppsala University Hospital for their contributions to the study. Data included in this paper were presented at the annual meeting of the Society of Nuclear Medicine and Molecular Imaging, June 8–12, 2013.

REFERENCES

1. Hughes AJ, Daniel SE, Kilford L, Lees AJ. Accuracy of clinical diagnosis of idiopathic Parkinson's disease: a clinico-pathological study of 100 cases. *J Neurol Neurosurg Psychiatry*. 1992;55:181–184.
2. Meara J, Bhowmick BK, Hobson P. Accuracy of diagnosis in patients with presumed Parkinson's disease. *Age Ageing*. 1999;28:99–102.
3. Catafau AM, Tolosa E. Impact of dopamine transporter SPECT using ¹²³I-ioflupane on diagnosis and management of patients with clinically uncertain Parkinsonian syndromes. *Mov Disord*. 2004;19:1175–1182.
4. Cummings JL, Henchcliffe C, Schaefer S, Simuni T, Waxman A, Kemp P. The role of dopaminergic imaging in patients with symptoms of dopaminergic system neurodegeneration. *Brain*. 2011;134:3146–3166.
5. Booij J, Knol RJ. SPECT imaging of the dopaminergic system in (premotor) Parkinson's disease. *Parkinsonism Relat Disord*. 2007;13(suppl 3):S425–S428.
6. Eckert T, Edwards C. The application of network mapping in differential diagnosis of Parkinsonian disorders. *Clin Neurosci Res*. 2007;6:359–366.
7. Brooks DJ. Imaging approaches to Parkinson disease. *J Nucl Med*. 2010;51:596–609.
8. Darcourt J, Booij J, Tatsch K, et al. EANM procedure guidelines for brain neurotransmission SPECT using ¹²³I-labelled dopamine transporter ligands, version 2. *Eur J Nucl Med Mol Imaging*. 2010;37:443–450.
9. Kapucu OL, Nobili F, Varrone A, et al. EANM procedure guideline for brain perfusion SPECT using ^{99m}Tc-labelled radiopharmaceuticals, version 2. *Eur J Nucl Med Mol Imaging*. 2009;36:2093–2102.
10. Eidelberg D, Moeller JR, Dhawan V, et al. The metabolic topography of parkinsonism. *J Cereb Blood Flow Metab*. 1994;14:783–801.
11. Eckert T, Feigin A, Lewis DE, Dhawan V, Frucht S, Eidelberg D. Regional metabolic changes in parkinsonian patients with normal dopaminergic imaging. *Mov Disord*. 2007;22:167–173.
12. Teune LK, Bartels AL, de Jong BM, et al. Typical cerebral metabolic patterns in neurodegenerative brain diseases. *Mov Disord*. 2010;25:2395–2404.
13. Nikolaus S, Antke C, Müller HW. In vivo imaging of synaptic function in the central nervous system: I. Movement disorders and dementia. *Behav Brain Res*. 2009;204:1–31.
14. Emond P, Guilloteau D, Chalon S. PE2I: a radiopharmaceutical for in vivo exploration of the dopamine transporter. *CNS Neurosci Ther*. 2008;14:47–64.
15. Emond P, Garreau L, Chalon S, et al. Synthesis and ligand binding of nortropine derivatives: N-substituted 2beta-carbomethoxy-3beta-(4'-iodophenyl)nortropine and N-(3-iodoprop-(2E)-enyl)-2beta-carbomethoxy-3beta-(3',4'-disubstituted phenyl)nortropine: new high-affinity and selective compounds for the dopamine transporter. *J Med Chem*. 1997;40:1366–1372.
16. Ziebell M, Holm-Hansen S, Thomsen G, et al. Serotonin transporters in dopamine transporter imaging: a head-to-head comparison of dopamine transporter SPECT radioligands ¹²³I-FP-CIT and ¹²³I-PE2I. *J Nucl Med*. 2010;51:1885–1891.
17. Jucaite A, Fernell E, Halldin C, Forsberg H, Farde L. Reduced midbrain dopamine transporter binding in male adolescents with attention-deficit/hyperactivity disorder: association between striatal dopamine markers and motor hyperactivity. *Biol Psychiatry*. 2005;57:229–238.
18. Ciumas C, Wahlin TB, Jucaite A, Lindstrom P, Halldin C, Savic I. Reduced dopamine transporter binding in patients with juvenile myoclonic epilepsy. *Neurology*. 2008;71:788–794.
19. DeLorenzo C, Lichenstein S, Schaefer K, et al. SEP-225289 serotonin and dopamine transporter occupancy: a PET study. *J Nucl Med*. 2011;52:1150–1155.
20. Zheng M, Appel L, Luo F, et al. Safety, pharmacokinetic, and positron emission tomography evaluation of serotonin and dopamine transporter occupancy following multiple-dose administration of the triple monoamine reuptake inhibitor BMS-820836. *Psychopharmacology (Berl)*. August 14, 2014 [Epub ahead of print].
21. Hirvonen J, Johansson J, Teräs M, et al. Measurement of striatal and extrastriatal dopamine transporter binding with high-resolution PET and [¹¹C]PE2I: quantitative modeling and test-retest reproducibility. *J Cereb Blood Flow Metab*. 2008;28:1059–1069.
22. DeLorenzo C, Kumar JSD, Zanderigo F, Mann JJ, Parsey RV. Modeling considerations for in vivo quantification of the dopamine transporter using [¹¹C]PE2I and positron emission tomography. *J Cereb Blood Flow Metab*. 2009;29:1332–1345.
23. Jonasson M, Appel L, Engman J, et al. Validation of parametric methods for [¹¹C]PE2I positron emission tomography. *Neuroimage*. 2013;74:172–178.
24. Lammertsma AA, Hume SP. Simplified reference tissue model for PET receptor studies. *Neuroimage*. 1996;4:153–158.
25. Gunn RN, Lammertsma AA, Hume SP, Cunningham VJ. Parametric imaging of ligand-receptor binding in PET using a simplified reference region model. *Neuroimage*. 1997;6:279–287.
26. Svarer C, Madsen K, Hasselbalch SG, et al. MR-based automatic delineation of volumes of interest in human brain PET images using probability maps. *Neuroimage*. 2005;24:969–979.
27. Koch W, Radau PE, Hamann C, Tatsch K. Clinical testing of an optimized software solution for an automated, observer-independent evaluation of dopamine transporter SPECT studies. *J Nucl Med*. 2005;46:1109–1118.
28. Litvan I, Agid Y, Calne D, et al. Clinical research criteria for the diagnosis of progressive supranuclear palsy (Steele-Richardson-Olszewski syndrome): report of the NINDS-SPSP international workshop. *Neurology*. 1996;47:1–9.
29. Gelb DJ, Oliver E, Gilman S. Diagnostic criteria for Parkinson disease. *Arch Neurol*. 1999;56:33–39.
30. Boeve BF, Lang AE, Litvan I. Corticobasal degeneration and its relationship to progressive supranuclear palsy and frontotemporal dementia. *Ann Neurol*. 2003;54(suppl 5):S15–S19.
31. McKeith IG, Dickson DW, Lowe J, et al. Diagnosis and management of dementia with Lewy bodies: third report of the DLB Consortium. *Neurology*. 2005;65:1863–1872.
32. Gilman S, Wenning GK, Low PA, et al. Second consensus statement on the diagnosis of multiple system atrophy. *Neurology*. 2008;71:670–676.
33. Lees AJ, Hardy J, Revesz T. Parkinson's disease. *Lancet*. 2009;373:2055–2066.
34. Meyer PT, Hellwig S, Amtage F. Dual-biomarker imaging of regional cerebral amyloid load and neuronal activity in dementia with PET and ¹¹C-labeled Pittsburgh compound B. *J Nucl Med*. 2011;52:393–400.
35. Gur RC, Ragland JD, Reivich M, Greenberg JH, Alavi A, Gur RE. Regional differences in the coupling between resting cerebral blood flow and metabolism may indicate action preparedness as a default state. *Cereb Cortex*. 2009;19:375–382.
36. Yaqub M, van Berckel BN, Schuitmaker A, et al. Optimization of supervised cluster analysis for extracting reference tissue input curves in (R)-[¹¹C]PK11195 brain PET studies. *J Cereb Blood Flow Metab*. 2012;32:1600–1608.
37. Varrone A, Asenbaum S, Vander Borgh T, et al. European Association of Nuclear Medicine Neuroimaging Committee. EANM procedure guidelines for PET brain imaging using [¹⁸F]FDG, version 2. *Eur J Nucl Med Mol Imaging*. 2010;36:2103–2110.
38. Ribeiro MJ, Ricard M, Lièvre MA, et al. Whole-body distribution and radiation dosimetry of the dopamine transporter radioligand [¹¹C]PE2I in healthy volunteers. *Nucl Med Biol*. 2007;34:465–470.
39. Guttman M, Stewart D, Hussey D, Wilson A, Houle S, Kish S. Influence of L-dopa and pramipexole on striatal dopamine transporter in early PD. *Neurology*. 2001;56:1559–1564.
40. Booij J, de Jong J, de Bruin K, et al. Quantification of striatal dopamine transporters with ¹²³I-FP-CIT SPECT is influenced by the selective serotonin reuptake inhibitor paroxetine: a double-blind, placebo-controlled, crossover study in healthy control subjects. *J Nucl Med*. 2007;48:359–366.